

FORMATION OF COLLOIDAL DISPERSIONS FROM SUPERSATURATED IRON(III) NITRATE SOLUTIONS. III. DEVELOPMENT OF GOETHITE AT ROOM TEMPERATURE

J.H.A. VAN DER WOUDE, P.L. DE BRUYN*

Van 't Hoff laboratory, State University of Utrecht, Transitorium 3, Padualaan 8, 3584 CH Utrecht (The Netherlands)

and J. PIETERS

Department of Molecular Cellbiology, State University of Utrecht, Transitorium 3, Padualaan 8, 3584 CH Utrecht (The Netherlands)

(Received 20 June 1983; accepted in final form 3 October 1983)

ABSTRACT

The development of colloidal goethite from partially neutralized iron(III) nitrate solutions has been investigated by high resolution electronmicroscopy and ultracentrifuge analysis. Monocrystalline rod-like particles characterized by (001) faces and very flat (010) and (120) faces are observed to form. Within these crystals, a substructure of oriented bundles of needles packed in the [001] direction are also identified. The needles have a typical diameter of 3 nm similar to that of the aged amorphous particle which first forms from the supersaturated solution.

It is shown that the needles can form both by oriented coagulation followed by recrystallization and by growth of an amorphous particle in the [001] direction through uptake of low molecular species from the solution.

The mechanism by which the rod-like particles form from the needles is not clear, but probably does not involve oriented coagulation of the acicular crystals. The final size of the goethite particles is determined by the initial supersaturation of the solution with respect to the amorphous phase. Ionic strength has a large influence on the sol stability.

INTRODUCTION

In two previous studies [1, 2] we investigated the kinetics of formation of an amorphous iron(III) hydroxide solid phase from acid iron(III) nitrate solutions by means of pH stat and free relaxation techniques. The amorphous colloidal particles in the prepared colloidal solutions were observed to transform eventually into a crystalline phase goethite at room temperature. The precursor role of these (amorphous) primary particles in the formation of the thermodynamically stable solid phase was convincingly established.

Until now no detailed study of the relation between the morphological

*To whom correspondence should be addressed.

development of goethite in a colloidal solution undergoing aging and the degree of neutralization of an iron(III) solution which gave birth to this sol, has been attempted. It is the intent of this paper to report on the results of such an investigation. We rely mainly on information obtained by high resolution electron microscopy (EM) and the ultra-centrifuge (UC) over aging periods of the order of one year or more. In the past, EM studies have proved useful in obtaining structural information about the various iron(III) hydrous oxide phases that may form from solution [3-9].

From the experimental observations we shall try to reconstruct the path along which formation of the larger goethite crystals from the smaller amorphous primary particles occurs.

EXPERIMENTAL

Preparation of sols

Two types of sols (A and B) were prepared by the homogeneous base titration [1, 10] of an acidified iron(III) nitrate solution. Sol A was obtained by titrating a $6.25 \times 10^{-3} M$ iron(III) nitrate solution with a 2.5 N NaOH solution at a rate of 10 meq/l h. By this procedure four sols (A_1 to A_4) were made. These sols are distinguished by the pH value (pH_0) at which the relaxation was started (see Table 1). Sol B was prepared by titrating a $6.25 \times 10^{-2} M$ iron(III) nitrate solution with the same base solution at 100 meq/l h up to a pH_0 of 1.96 before starting the relaxation which initiates the formation

TABLE 1

Characteristic features of sol preparation

	Sol A (from $6.25 \times 10^{-3} M$ solution)				Sol B (from $6.25 \times 10^{-2} M$ solution)
	A_1	A_2	A_3	A_4	
<i>Conditions at start of free relaxation</i>					
pH_0	2.21	2.33	2.49	2.64	1.96
$(OH/Fe)_0$	0.30	0.44	0.84	1.61	0.30
induction time t_i (h)	135	22	~0	0	65
<i>Conditions after one year of aging</i>					
pH	1.95	1.96	2.03	2.20	1.51
OH/Fe	1.25	1.70	2.36	2.41	0.70
Ionic Strength (M)	0.09	0.085	0.08	0.078	0.44
specific surface (m^2/g)	44	—	—	—	130

of the colloidal phase. The important features of the relaxation behavior are also summarized in Table 1. The OH/Fe ratio in this table at which the relaxation started is the amount of hydroxyl ions taken up by the system per total amount of iron after correcting for the amount needed to reach the desired pH₀.

The OH/Fe ratio after one year of aging is determined by adding to the amount of OH⁻ already bound to iron(III) at the start of the free relaxation — the additional amount of OH⁻ consumed during aging. This amount is assumed to be equal to the observed quantity of H⁺ released to the solution. As the OH/Fe ratio in the solid phase would be approximately 3, the fraction of the total iron in the solid phase will be about 30% in sol A₁ and 50% in sol A₂ after one year. In the case of sols A₃ and A₄ we may conclude that most of the iron is present in the solid phase. At the low pH values of the solutions one would expect the soluble species to be mostly hydrated iron cations. In sol B a flocculated sediment formed within two weeks whereas all four of the A type sols remained stable.

Measurement techniques

a. Electronmicroscope

The solid particles were viewed in a JEM 200 C electronmicroscope equipped with an eucentric side-entry goniometer, in order to perform tilting experiments, and also in a Philips EM 301 unit equipped with a standard biological stage and a TV camera with image intensifier. The sol was spread with a nebulizer on standard 100 mesh EM grids. To improve the hydrophilic nature of the support films, the grids were exposed to a glow discharge in an argon atmosphere (about 0.05 torr) for about 3 min. This procedure improves the spreading of the sol droplets.

Samples were first studied in the JEM 200 C. Attempts to obtain a stereoscopic view failed because diffraction contrast disturbed the operation. Attempts were also made to get, by tilting, an image of the faces of the particles perpendicular to their longitudinal axis. In spite of a tilting angle of $\pm 60^\circ$ this succeeded only when clusters of particles were present. Furthermore, although the lattice resolution of the JEM is better than 4.5 Å, for practical reasons it was not possible to achieve this. When high resolution was desired we used the Philips EM 301 even though it lacked tilting facilities. In order to view the particles in this microscope in different orientations, the sol was spread in large quantities on the grid. Electron diffraction patterns were also taken. Evaporated TiCl was used as an internal standard.

b. Ultracentrifuge (UC)

Sedimentation measurements were performed in a Beckmann Spinco model E ultracentrifuge by applying the scan method. The sedimentation rate of the particles was measured with the aid of a UVV spectrometer. This was done by adjusting the wavelength to obtain full scale absorption at the

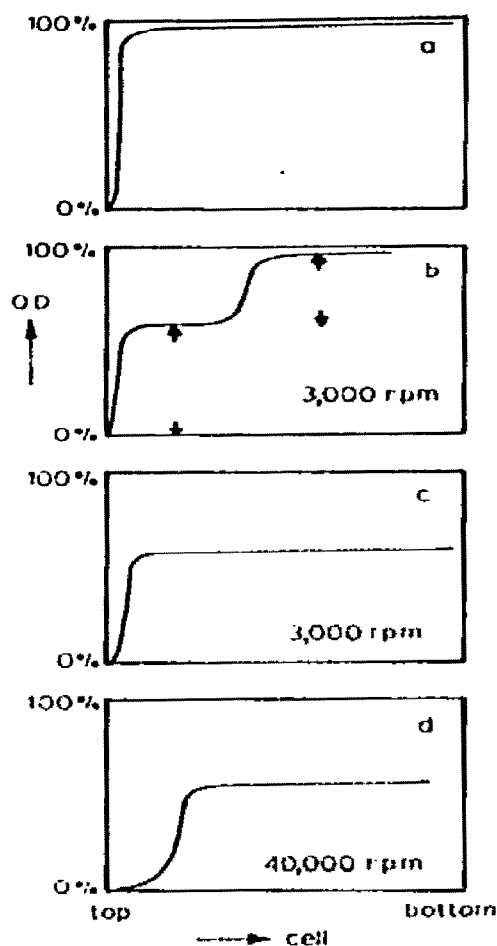


Fig. 1. A schematic representation of UC scan patterns of a sol consisting of two types of particles of distinctly different size (heavy and light particles). (a) Adjustment of the wavelength at the start of the sedimentation run to give optimal absorbance. (b) The heavy particle sediments at low centrifugal force. The approximate relative concentrations of the heavy and light particles are indicated with arrows. (c) The heavy component has sedimented to the bottom of the cell. (d) The light component sediments at high centrifugal force.

start of the run. The optical density (OD), as a function of the cell length, served as a measure of particle concentration and was followed as a function of time. Particles of different sizes could be detected in one run and their relative concentrations evaluated as illustrated in Fig. 1. At the start of the sedimentation run of a sample of known aging time the wavelength is adjusted to give optimal absorbance (Fig. 1a). Assuming two types of particles of distinctly different size to be present in detectable amounts, the largest ones will begin to sediment at low centrifugal force (Fig. 1b). From this

scan pattern the approximate relative concentrations of heavy and light particles can be determined in addition to the sedimentation coefficient of the heaviest component. On continuing the run, the heaviest component will sediment to the bottom of the cell and, on increasing the centrifugal force, the sedimentation coefficient of the lighter particles can be determined (Fig. 1c, d).

c. Auxiliary techniques

Samples of the solid particles in sol A₁ were obtained by centrifuging at 10,000 rpm. These samples, and also B precipitates, were thoroughly washed and dried at 60°C. X-Ray diffraction analyses and IR spectra were taken of the dried samples. The specific surfaces of the A₁ and B particles were measured in a Quanta sorb apparatus by utilizing the three point BET method with nitrogen as adsorbate.

RESULTS

UC measurements

Information about the sedimentation behavior with changing aging time of the sols under investigation is summarized in Table 2. S₂₀ measurements on type A sols indicate the simultaneous presence of two types of particles of different sizes during most of the aging time. For convenience and to indicate the order of their appearance, we refer to the smaller particle as the primary particle and the larger as the secondary particle. These two types of particles have also been noted by Dousma and De Bruyn [11]. It should

TABLE 2

Changes in sedimentation coefficient and particle size with aging time

Aging time	A ₁		A ₂		A ₃		A ₄		B	
	EM (A)		EM (A)		EM (A)		EM (A)		EM (A)	
	S ₂₀ (S)	l × w*	S ₂₀ (S)	l × w	S ₂₀ (S)	l × w	S ₂₀ (S)	l × w	S ₂₀ (S)	l × w
1 day	a	a	a	—	10	—	12	—	a	a
3 days	a	a	21	—	—	—	14.5	—	—	—
8 days	314	—	280/26 ^b	—	21	—	13	—	280	—
12 days	—	670 300	—	—	—	—	—	—	d	560 330
15 days	2400	—	—	—	—	—	—	—	—	—
30 days	—	—	470/23	—	230/19	—	16	—	—	—
52 days	—	765 320	—	460 100	—	320 70	—	500 50	—	—
6 months	2200	800 320	640/c	490 150	375/26	660 110	280/25	—	—	—
11 months	2560	800 320	715/c	—	410/c	—	317/c	500 50	—	—
2 years	2500	800 320	—	500 150	—	—	—	—	—	—

a. No particles were detected.

b. Two distinct types of particles present.

c. The primary particle concentration drops below the detection limit.

d. Flocculation.

*l = length, w = width.

be noted that although the primary particle could not be detected in sol A_1 , its presence was verified by EM measurements. The primary particle is the amorphous precursor which was studied in previous investigations [1, 2]. It is seen to reach a constant S_{20} value of 25 S with aging time and then to disappear at high aging times from the colloidal solution. The larger secondary particle is seen to appear quite early in the aging sol A_1 and to reach a constant size after two weeks as expressed by an S_{20} value of 2500 ± 100 Svedbergs. From the scan pattern a narrow particle size distribution is indicated. These secondary particles appear later during the aging time in the sol sequence A_1 to A_4 . The higher the initial pH_0 (see Table 1) the smaller the average S_{20} value of the secondary particle and the broader the particle size distribution. As mentioned earlier, these sols remained stable over a period of years. After a long induction period (see Table 1) sol B particles were observed to grow rapidly and flocculation set in after two weeks of aging. The information obtainable from UC measurements on this sol is thereby limited.

As discussed in the experimental section, UC scan experiments can yield information about the nature of the dispersed phase in a sol during aging. In Fig. 2 the approximate fractions of the total absorption in the scan pattern due to primary and secondary particles are plotted as a function of the logarithm of time for sols A_2 , A_3 and A_4 . Above the plots we give the wave lengths at which the OD measurements were done. Two important aspects of the aging behavior are revealed in this Figure. First, regardless of the initial pH_0 (or OH/Fe ratio) the concentration of the primary particles is seen to decrease with increase in aging time. Second, to obtain full scale absorption in the scan measurements it was necessary to increase the wavelength with increasing time of aging in sols A_2 and A_3 (see Fig. 2a, b), whereas in sol A_4 this was not necessary. This adjustment in wavelength was

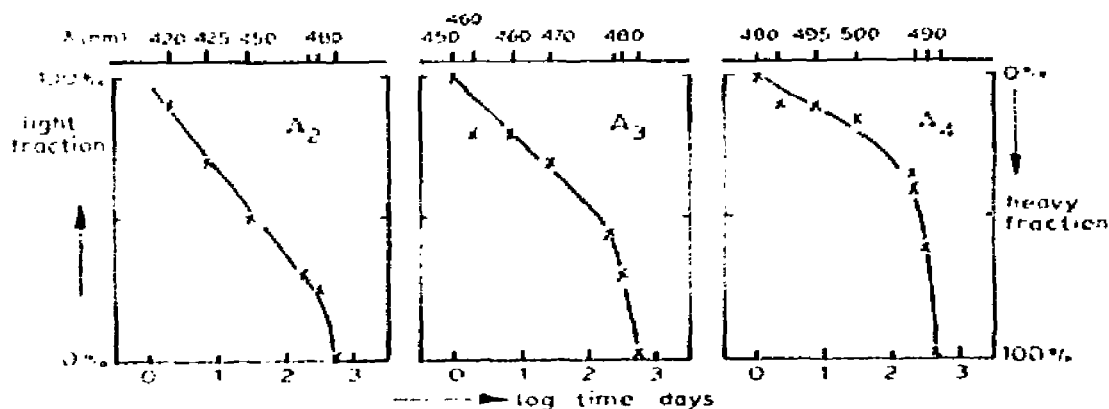


Fig. 2. The approximate fraction of the total absorption in the scan pattern due to primary and secondary particles as a function of the logarithm of time for sols A_1 , A_2 and A_4 (see Table 1). The wavelengths at which the UC measurements were done are given at the top of the figures.

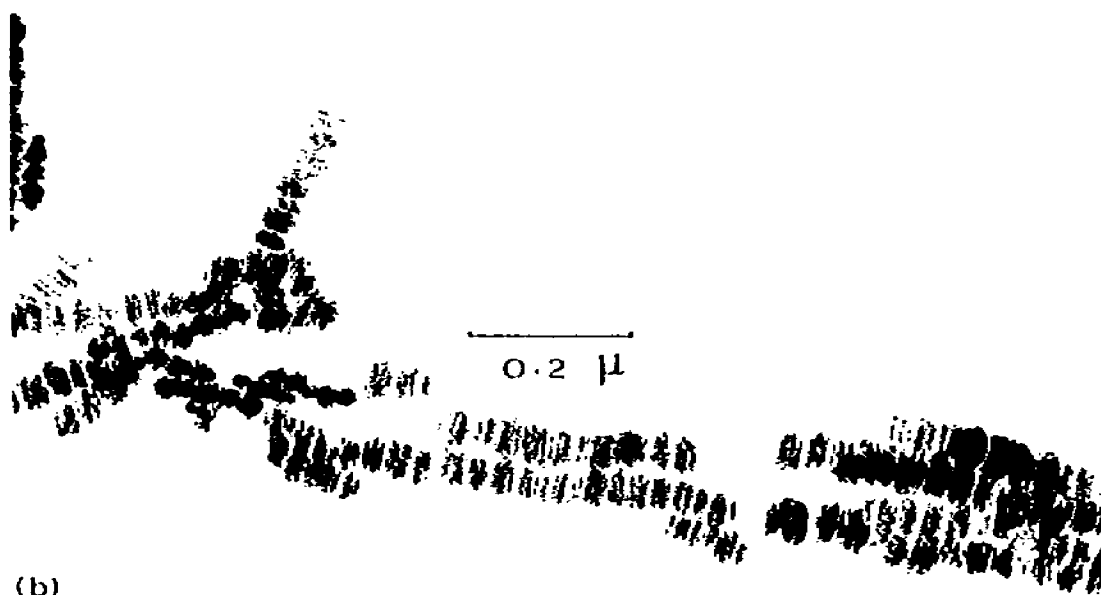
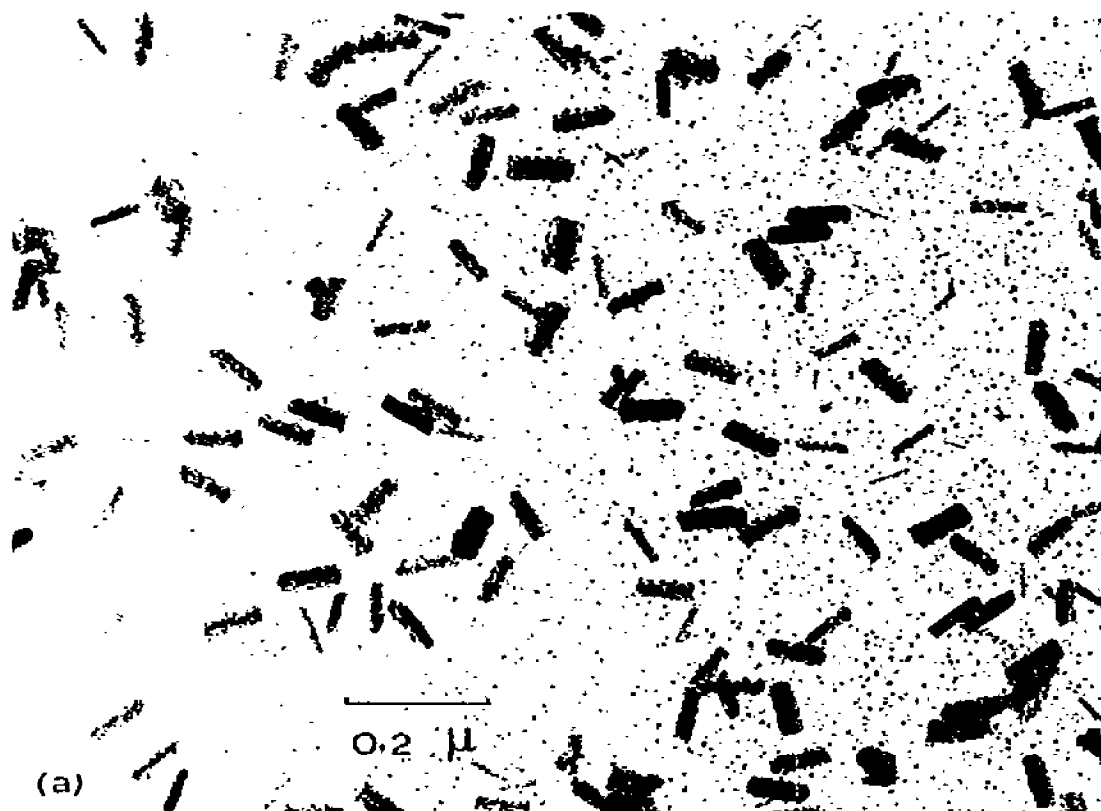
greater for sol A₂ than for sol A₃. As the absorption spectrum of an iron hydroxide sol shows a monotonic decrease of the absorption in the visible region of the spectrum with increasing wavelength, this second observation implies that on aging the total amount of iron(III) in the solid phase in sols A₂ and A₃ must have increased and must have remained nearly constant in sol A₄. We may therefore conclude from these results that the primary particles are consumed by growing secondary (goethite) particles but that the latter also grow by extracting low molecular weight, non-absorbing species from the solution phase. The observed constant S_{20} value (see Table 2) of the primary particles in the presence of secondary particles clearly demonstrates that the former are not involved in the reaction with soluble solution species. The indicated growth of secondary particles in sol A₄, almost entirely due to consumption of primary particles, is, of course, consistent with the path followed in the precipitation diagram [1]. Nearly all the iron(III) in the solution will have been depleted in the formation of the amorphous primary particle because of the higher initial pH of relaxation compared to, for example, the lower starting pH in the case of sol A₁.

EM results

EM studies also revealed the presence of primary and secondary particles as may be seen in Fig. 3a which is an electronmicrograph of sol A₁ after aging for one year. Within a few days following an induction time, the primary and a much larger secondary particle are seen when viewing sol A₁ and sol B in the electronmicroscope. In the beginning stage (after about 12 days of aging) the secondary particles in sol A₁ are somewhat ellipsoidal in shape, but later on they become rectangular and rather uniform in size (see Fig. 3a). They reach an ultimate size of $800 \pm 50 \text{ \AA}$ by $320 \pm 30 \text{ \AA}$ as shown in Table 2. In sols A₂, A₃ and A₄ these two types of particles are also detected. The secondary particles, however, reach a smaller ultimate size than those in sol A₁ (see Table 2). Furthermore the ratio of particle length to width increases with increasing pH₀ of relaxation (see Table 1). As already noted in the presentation of the UC results, the uniformity in the particle size is also seen to decrease from aged sol A₁ to aged sol A₄.

Strings of particles linked together side-wise are the most characteristic features noted when viewing sol B in the EM (see Fig. 3b). This observation was also made by Dousma and De Bruyn [11] in their study of the formation of goethite from $6.25 \times 10^{-2} \text{ M}$ Fe(III) solutions. We note from Fig. 3b and other similar pictures that the strings are composed of maximally 30 subunits which are again quite rectangular in shape with length $560 \pm 50 \text{ \AA}$ and width $330 \pm 50 \text{ \AA}$. These (flocculated) subunits are identical to the (dispersed) secondary particles noted in type A sols. Their contours are, however, not as smooth as those observed in sol A₁. The B particles* are observed

*The secondary particles in sols A and B will from now on be referred to as simply A and B particles.



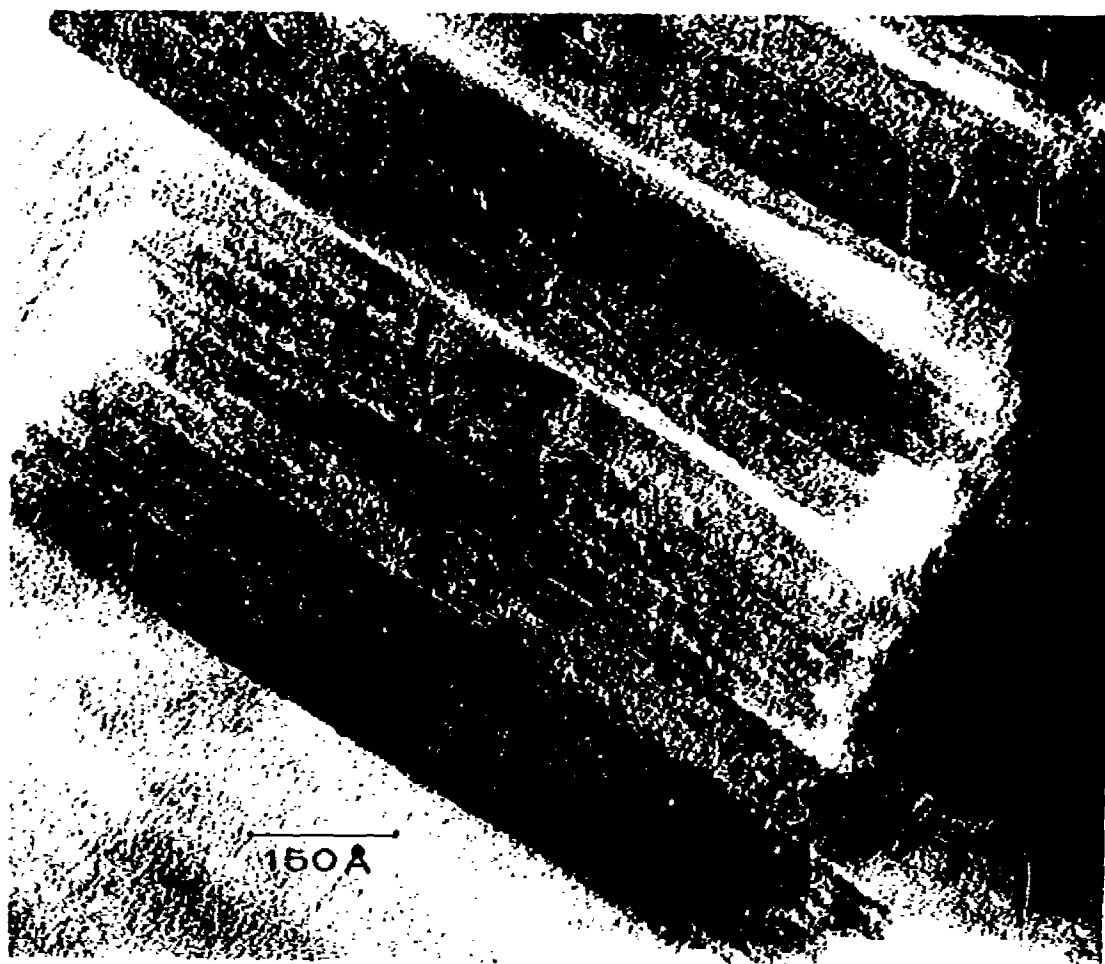


Fig. 4. High resolution electron micrograph of sol A₁. The fringes parallel to the longitudinal direction of the particles are 4.6 ± 0.5 Å apart.

to show a two-dimensional granular structure resembling a regular orientation of lath-shaped units parallel to their long dimension. The width of these units is 30–40 Å which is the same linear dimension of the primary particle. This observation provides a valuable clue when one attempts to reconstruct the aging process.

X-ray diffraction and electron diffraction show that both A and B particles are goethite crystals.

Fig. 3. (a) Electronmicrograph of sol A₁ (see Table 1) after one year of aging showing the primary and secondary particles. (b) Electronmicrograph of sol B (see Table 1) depicting strings of laterally linked particles.

High resolution EM studies uncover a very regular internal structure of A_1 particles as is shown in Fig. 4. Parallel to the longitudinal direction of the particles, fringes are clearly visible with a periodicity of $4.6 \pm 0.5 \text{ \AA}$. This observation indicates these particles to be monocrystalline and thus highly crystalline. A two-dimensional granular structure already referred to is, however, also noticeable. It would therefore appear that in three dimensions the indicated "single" crystals are composed of needle-like subdivisions with a thickness of about 30 \AA . This substructure is especially clearly visible near the extremities of the crystals. Of importance is also the lateral, side by side orientation of the A particles as shown in Fig. 4. We believe this behavior to express a preferred orientation when individual A particles are forced to approach one another during flocculation. Figure 5 which depicts an A_1 sol that was flocculated prior to being sprayed on the grid for viewing in the EM, corroborates this contention. Slow flocculation was induced by dialyzing the sol against a solution of the same pH but with a slightly higher concentration of indifferent electrolyte ($0.2 M \text{ NaNO}_3$).

Examples of the particle faces perpendicular to the longitudinal crystal axis, obtained in the EM 301 and by tilting the grid in the JEM 200 C, are shown in Fig. 6. It was noticed that a small change in the tilting angle of about one degree caused a fading of the sharp outline of these faces. This observation indicates the crystal faces lying parallel to the longitudinal axis to be very flat. The cross-sections of the A_1 particles have a characteristic diamond-like shape with an acute angle of $47 \pm 1^\circ$. Often irregular edges are

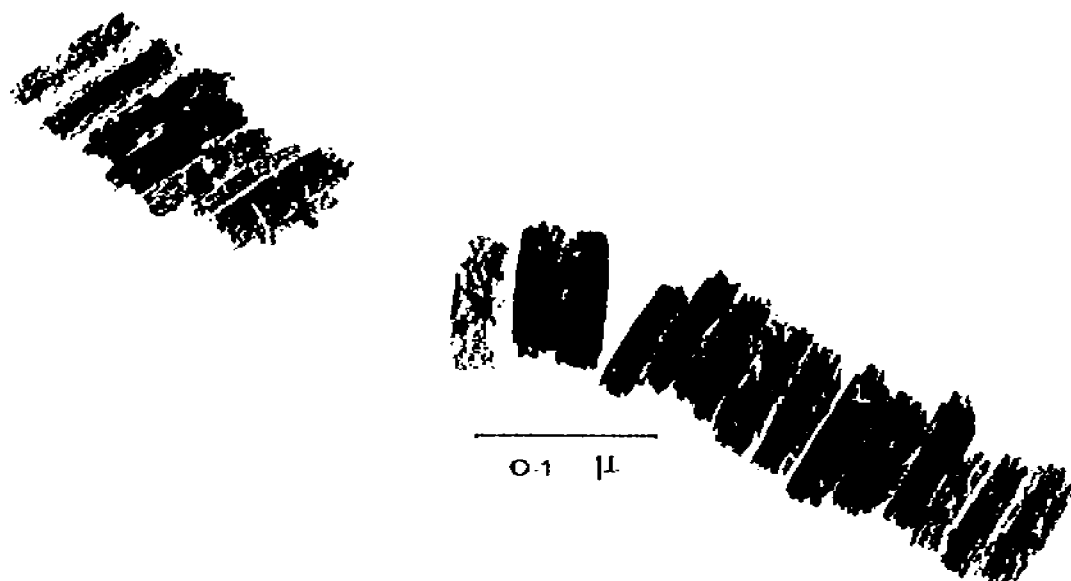


Fig. 5. Electronmicrograph of an A_1 sol that was flocculated prior to being sprayed on the grid.

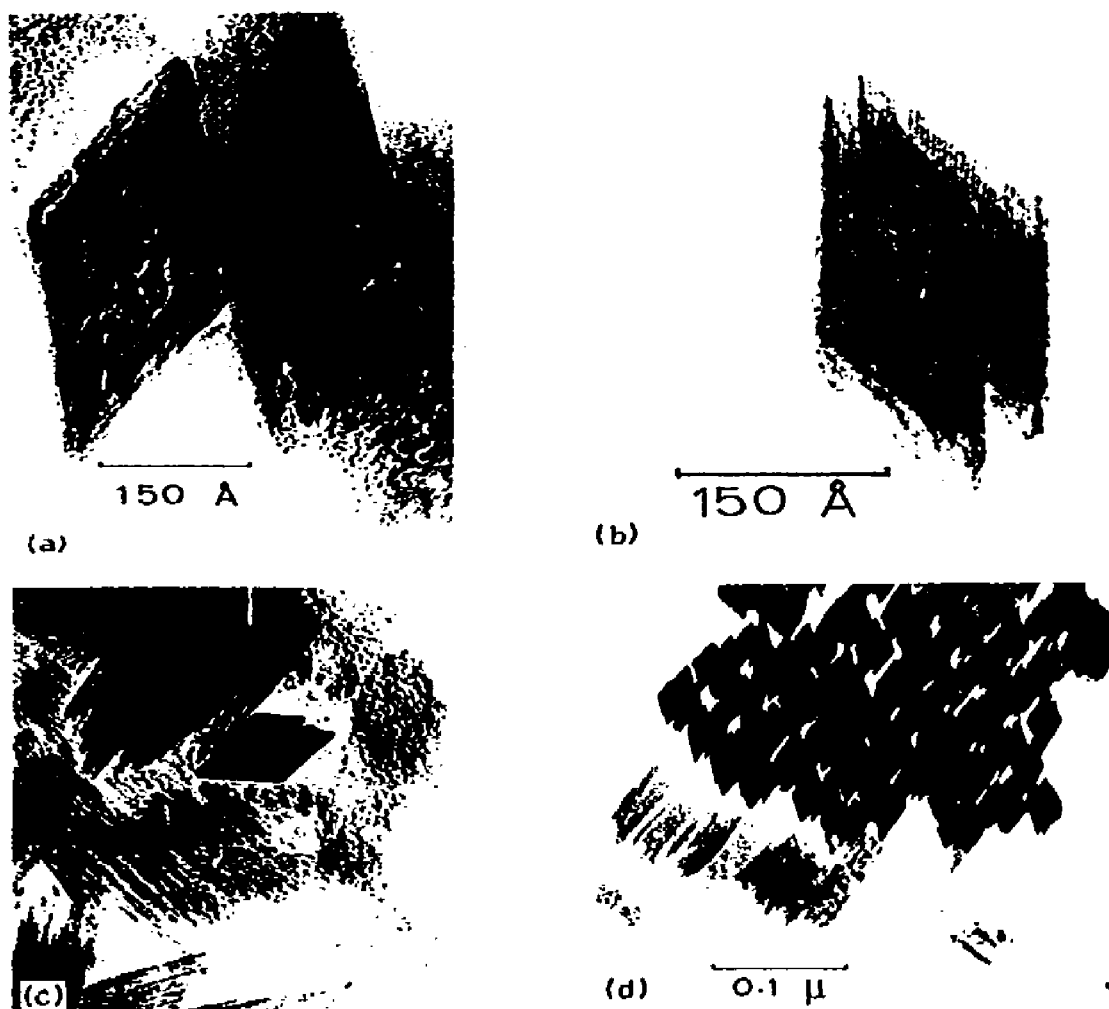


Fig. 6. Electronmicrographs of the faces perpendicular to the longitudinal axis of particles of an A_1 sol. The characteristic diamond-like shape with an acute angle of $47 \pm 1^\circ$ of these crystal planes is clearly displayed. (a) Demonstrating fringes with separation of 4.5 \AA and parallel to one of the face edges. (b), (c) and (d) make clear that irrespective of irregularities of the edges, the acute angle of $47 \pm 1^\circ$ is retained. (d) Large clusters of A particles formed by preferential side by side flocculation are illustrated.

observed in the diamond-like faces (Fig. 6 b—d) while retaining this shape and the 47° angle. Fringes with a separation of about 4.5 \AA are also seen in these cross-sectional views of A particles (Fig. 6a, b), thus again confirming the highly crystalline nature of the solids. Figure 6d illustrates that large clusters of A particles form in the preferential side by side orientation in the flocculated state.

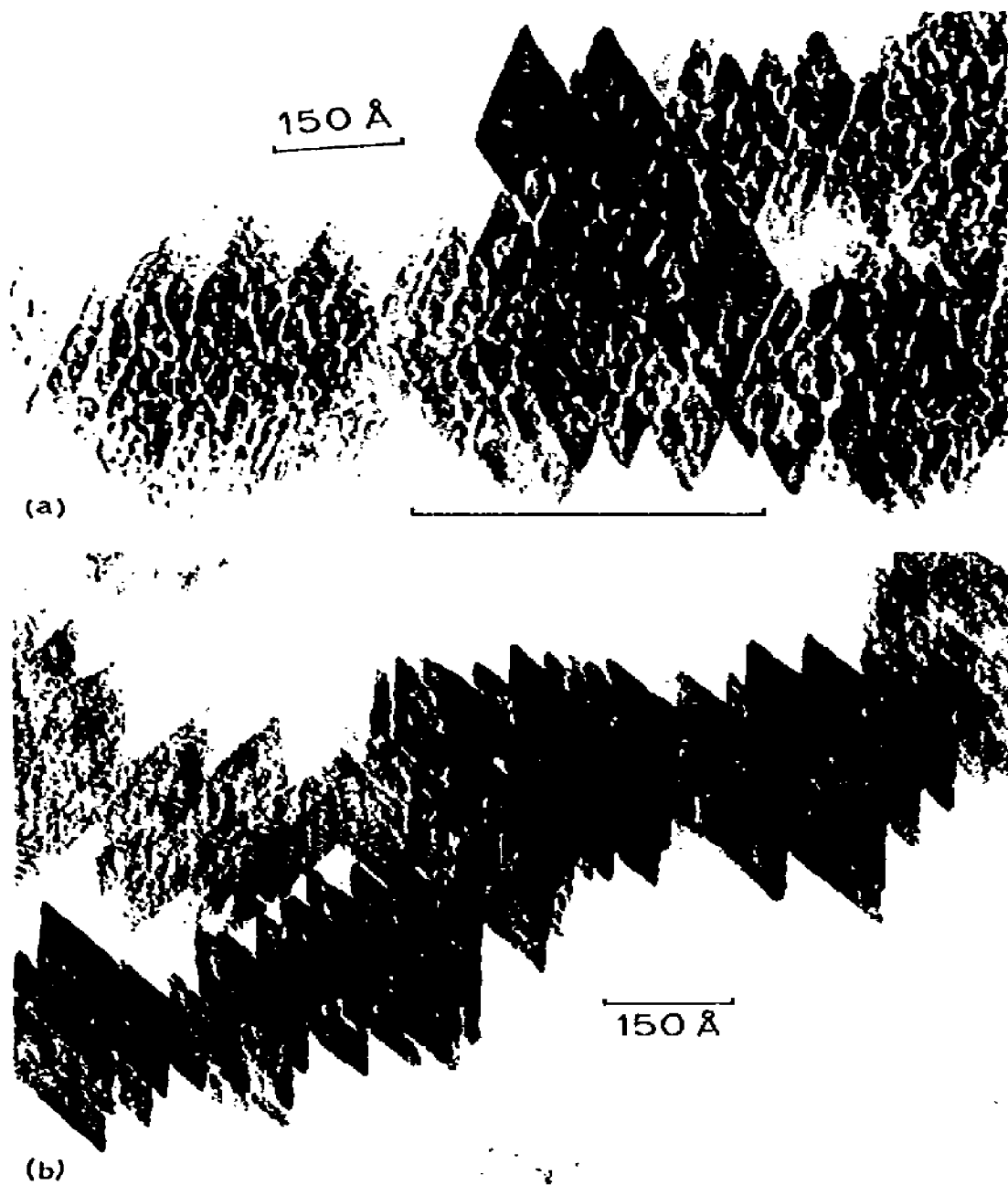


Fig. 7. Electronmicrographs of the faces of the B particles perpendicular to their longitudinal axis, again showing the diamond shape with an acute angle of $47 \pm 1^\circ$. In (a) the dimension of a B particle is indicated. (b) shows the interference pattern and the fringes parallel to one of the edges with a separation of $4.5 \pm 0.5 \text{ Å}$.

A typical view of the faces of B particles perpendicular to their longitudinal axes is presented in Fig. 7. We recall that these particles were already flocculated before being brought on the grid. These faces are not as regular in outline as those of the A₁ particles (Figs. 4 and 6) but the characteristic diamond-shapes with an acute angle of $47 \pm 1^\circ$ are again clearly visible (Fig. 7a). In the face may be seen small regions with linear dimensions of the order of 30 \AA , often oriented parallel to the edges, and also pores up to 10 \AA in diameter. Again the edges of the diamond-like faces are sharp, thus reflecting the flatness of the faces parallel to the long axis of the particle. In Fig. 7b fringes with a separation of $4.5 \pm 0.5 \text{ \AA}$ parallel to one of the edges of the diamond-like face are again clearly visible. This and the interference pattern in Fig. 7b prove that, in spite of the open structure, the B particles are highly crystalline.

In Fig. 8 we have attempted a schematic reconstruction of the characteristic features of the A and B particles as deduced from the electronmicrographs shown in Figs. 4, 6 and 7.

Both A and B particles have been shown to be goethite and, according to the EM studies, have identical crystal habits. Goethite is orthorhombic with

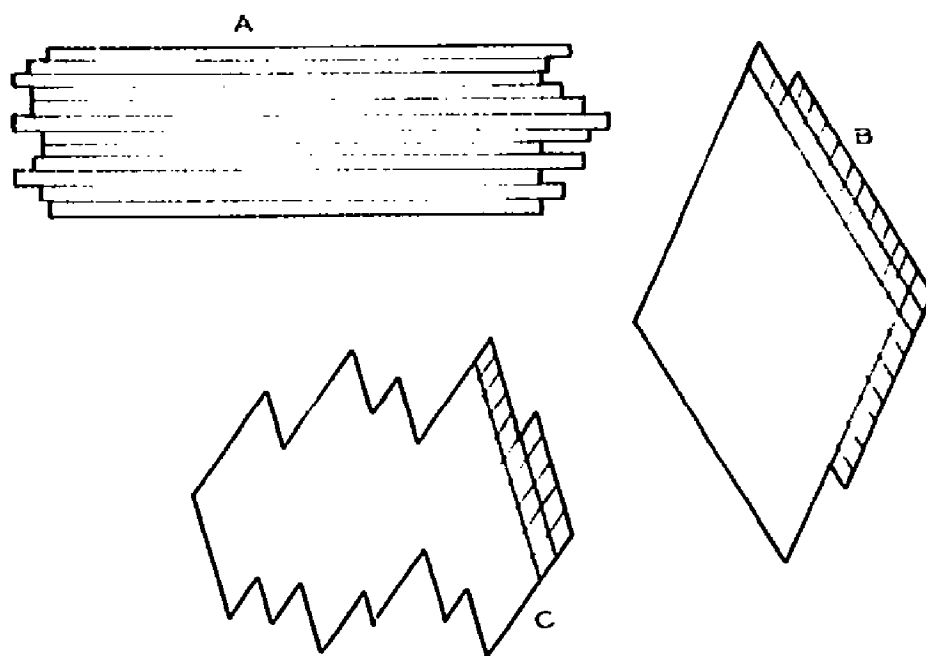


Fig. 8. Schematic reconstruction of the characteristic features of the secondary particles. (A) An A particle with the lath-shaped units parallel to their long dimension. The thickness of these units is $30\text{--}40 \text{ \AA}$. (B) View of the face of an A particle perpendicular to the longitudinal axis illustrating the needle-like subdivision. (C) Same as (B), but of a B particle illustrating the less regular outline, while retaining the $47 \pm 1^\circ$ angle.

hexagonal close-packing of oxygen atoms and with unit cell dimensions $a_0 = 4.6 \text{ \AA}$, $b_0 = 9.96 \text{ \AA}$, $c_0 = 30.2 \text{ \AA}$ and $Z = 4$ [12].

When this information is combined with that derived from the electron-micrographs we conclude that the diamond-shaped face, the (001) face, is bounded by the (010) and (120) faces. The separation of the observed fringes is in good agreement with the a_0 dimension of the unit cell.

In conclusion, it is interesting to establish to what extent the information on particle size contained in the UC measurements is in agreement with that derived from the EM studies and summarized in Table 2. We approximate the shape of the particles by a prolate ellipsoid with the long and short axis equal to the length and width of the A particles as observed in the EM (see Table 2). Using the friction coefficient for ellipsoidal particles as derived by Perrin [13], a sedimentation coefficient may be calculated and compared with the observed one. Although the particles were shown to be crystalline, the EM study also showed them to contain voids (pores). Thus the density of the particles need not necessarily equal that of massive goethite (4.3 g/cm^3). On performing these calculations, assuming densities of 4.3 g/cm^3 and also 3.3 g/cm^3 , the following pairs of S_{20} values are predicted for the sols A_1 , A_2 and A_3 , respectively: (3200 S, 2240 S), (810 S, 560 S) and (550 S, 390 S). We note that the calculated values based on a density of about 3.3 g/cm^3 are in reasonable agreement with the measured sedimentation coefficients.

DISCUSSION

Aging of a fresh precipitate or newly formed colloidal solution may occur by way of a variety of secondary processes and may result in a change in structure and morphology of the primary precipitate. The processes responsible for this change may be classified as follows [14]: (a) perfection of the surface, (b) transformation of a metastable modification into a more stable one (Ostwald Rule of Stages), (c) Ostwald ripening or growth of larger particles at the expense of smaller ones and (d) aggregation of primary particles with subsequent recrystallization. In the system under investigation the contributions of processes (a), (b) and (d) are readily recognized but the aging behavior cannot be described as a classic example of Ostwald ripening.

UC and EM studies show that over a time span of about one year, small (5 nm) quite monodisperse amorphous particles are transformed into single crystals of goethite featuring rough (001) faces and smooth (010) and (120) faces. High resolution EM studies also reveal the crystals of goethite to be composed of acicular or needle-shaped subunits elongated in the [001] direction and approximately of the same thickness as the primary particles. The work of Naono and Fujiwara [8, 9] may be cited as support for this observed substructure of the goethite crystals. These investigators noted that needles of $\alpha\text{-Fe}_2\text{O}_3$ of 2 nm diameter separated by pores (8 Å) form when $\alpha\text{-FeOOH}$ and $\beta\text{-FeOOH}$ transform at 300°C in vacuo. Such a change

cannot be explained unless the needle-like units were originally present in the untransformed material. The size of the goethite crystals and the stability of the colloidal solution after aging depend on the pH of the relaxation experiment and the total iron(III) concentration.

The transformation from amorphous to goethite structures implies splitting-off of water and densification of the particles [15, 16]. Evidence will be presented in another publication that this aspect of the aging process must occur before the large secondary particles form. The details of the process by which an aged (goethite-like) primary particle grows to form reasonably uniformly-sized goethite crystals are difficult to reconstruct because of lack of information. From the UC study and a general consideration of the composition of the aging solutions in sols A_1 to A_4 , we deduce that the growth or formation of the acicular crystals (or sub-units) of thickness 3 nm, as observed in the EM investigation, may occur in two ways or a combination thereof.

One way will involve the growth of needles by incorporation of low molecular soluble Fe(III) species still available in the solution supersaturated with respect to goethite. The preferred growth direction will be the [001] direction. This mechanism will prevail in the A_1 type sol and will become increasingly less dominant in sols A_2 and A_3 (see Fig. 2).

The other "growth" mechanism will involve formation of the acicular sub-units by a process involving the stacking and cementing of aged primary particles in the [001] direction. This process resembles, and in fact may be identified as, an oriented coagulation phenomenon. Murphy et al. [5] claim to have observed this behavior in aged colloidal solutions with high initial OII/Fe ratios and Mackenzie and Meldau [3] observed this in gels at pH 5 and pH 10. The former authors claim to have detected goethite only after this arrangement had been realized and the latter investigators believe that in the early stages needles consist of primary particles cemented together in a row rather than existing as true crystals. This method of growth we believe is typical for sol A_4 in our experiments.

It is, however, the details of the growth process involving the conversion of these needle-like units (regardless of the way in which they were formed) to the final goethite crystals that have escaped our attention. This stage in the formation of the large secondary particles may again be accounted for by an oriented "coagulation" of the preformed needle-like crystals. The fact that we were unable to identify single needle-like "crystals" in the EM would argue against such a simple explanation. It is also difficult to account for the reasonable monodispersity of the goethite crystals by such a mechanism. An alternative explanation, which might be more consistent with some of the experimental observations, may be the initial clustering of primary particles round one or more needle-like crystals. Such a starting situation may account for the observation of ellipsoidal units in sol A_1 after 12 days of aging (see Table 2). However, insufficient information cautions us not to speculate too much about this stage in the aging process.

The formation of iron oxyhydroxide particles of acicular crystals is not limited to goethite structures. Watson et al. [6] reported akageneite (β -FeOOH) particles of length 150 nm and width 50 nm to be composed of subcrystals of ca. 3 nm diameter but with hollow cores.

The crystallographic orientation of the faces exposed to the equilibrium solution apparently depends on the temperature and pH. Thus, Atkinson et al. [17] mention the presence of (001), (010) and (100) crystal faces at high pH and temperature. Instead of the (100) crystal face we have observed that the (120) face develops.

In this study the importance of flocculation in colloidal iron(III) solutions has been amply demonstrated. The role of ionic strength on the stability of the sols is shown in Table 1. Sol B, formed at a higher ionic strength than sol A, rapidly flocculated whereas sol A remained stable. The role of preferred orientation and ionic strength on the flocculation behavior will be discussed in a subsequent publication.

ACKNOWLEDGMENT

Mr. J. Suurmond is thanked for making the ultracentrifuge measurements.

REFERENCES

- 1 J.H.A. Van der Woude and P.L. de Bruyn, *Colloids Surfaces*, 8 (1983) 55.
- 2 J.H.A. Van der Woude, P. Verhees and P.L. de Bruyn, *Colloids Surfaces*, 8 (1983) 79.
- 3 R.C. Mackenzie and R. Meldau, *Min. Mag.*, XXXIII (1959) 153.
- 4 W. Feitknecht and W. Michaelis, *Helv. Chim. Acta*, XLV (1962) 212.
- 5 P.J. Murphy, A.M. Posner and J.P. Quirk, *J. Colloid Interface Sci.*, 56 (1976) 312.
- 6 J.H.L. Watson, R.R. Cardell Jr. and W. Heller, *J. Phys. Chem.*, 66 (1962) 1757.
- 7 H. Naono and R. Fujiwara, *J. Colloid Interface Sci.*, 73 (1980) 406.
- 8 H. Naono, R. Fujiwara, H. Sugioka, K. Sumiya and H. Yanazawa, *J. Colloid Interface Sci.*, 87 (1982) 317.
- 9 R.J. Atkinson, A.M. Posner and J.P. Quirk, *J. Inorg. Nucl. Chem.*, 30 (1968) 2371.
- 10 J. Dousma and P.L. de Bruyn, *J. Colloid Interface Sci.*, 56 (1976) 527.
- 11 J. Dousma and P.L. de Bruyn, *J. Colloid Interface Sci.*, 64 (1978) 64.
- 12 C. Palache, H. Berman and C. Frondel, "The System" of Mineralogy of I.D. Dana and E.S. Dana, Yale Univ., Vol. 1, 7th ed., Wiley, New York, 1944.
- 13 J. Dousma, T.J. van den Hoven and P.L. de Bruyn, *J. Inorg. Nucl. Chem.*, 40 (1978) 1089.
- 14 I.M. Kolthoff, *Analyst*, 77 (1952) 1000.
- 15 J.J. Fripiat and M. Pennequin, *Bull. Soc. Chim. Fr.*, 6 (1965) 1655.
- 16 B.A. Sommer, D.W. Margerum, J. Renner, P. Saltman and Th.G. Spiro, *Bioinorg. Chem.*, 2 (1973) 295.
- 17 R.J. Atkinson, A.M. Posner and J.P. Quirk, *Clays Clay Miner.*, 25 (1977) 49.